

Unification of BKT and BEC Phase Transitions in a Trapped Two-Dimensional Bose Gas

Richard J. Fletcher^{*†}, Martin Robert-de-Saint-Vincent^{*‡},

Jay Man, Nir Navon, Robert P. Smith, Konrad Viebahn, and Zoran Hadzibabic

Cavendish Laboratory, University of Cambridge, J. J. Thomson Avenue, Cambridge CB3 0HE, United Kingdom

(Dated: December 3, 2024)

We study the critical point for the emergence of coherence in a harmonically trapped two-dimensional (2d) Bose gas with tuneable interactions. Over a wide range of interaction strengths we find excellent agreement with predictions based on the Berezinskii-Kosterlitz-Thouless (BKT) theory of 2d superfluidity. This allows us to quantitatively show, without any free parameters, that the interaction-driven BKT transition smoothly converges onto the purely statistical Bose-Einstein condensation (BEC) transition in the limit of vanishing interactions.

PACS numbers: 03.75.Hh, 67.85.-d

Reducing the dimensionality of a physical system increases the importance of thermal fluctuations and can profoundly affect the type of order that the system can display at low temperatures [1–4]. In a uniform two-dimensional (2d) Bose gas, the true long-range-order (LRO) associated with Bose-Einstein condensation (BEC) is precluded at any non-zero temperature by the Mermin-Wagner theorem. However, an interacting 2d Bose gas still undergoes the Berezinskii-Kosterlitz-Thouless (BKT) transition to a superfluid state at a critical phase-space density D_{BKT} [5, 6]. Specifically, classical-field Monte-Carlo simulations [7] predict $D_{\text{BKT}} = \ln(380/\tilde{g})$, where \tilde{g} is a dimensionless measure of the interaction strength [8]. This result makes it manifest that the transition is interaction driven; the critical temperature, $T_c \propto n/D_{\text{BKT}}$, where n is the gas density, vanishes in the non-interacting limit, $\tilde{g} \rightarrow 0$, for any non-infinite n . While for phase-space density $D > D_{\text{BKT}}$ true LRO is still absent, the first order correlation function, $g_1(r)$, decays only algebraically at large distance, in contrast to the exponential decay in the normal degenerate gas. Such extended coherence is sufficient for superfluidity [9], and in practice offers a signature of the phase transition [10–13].

In contrast to the infinite uniform system, in a 2d harmonic trap, pertinent to most ultracold-atom experiments on BKT physics [14–28], the modified density of states allows for a BEC transition to occur in the ideal gas ($\tilde{g} = 0$). In an isotropic trap of frequency ω_r , it should occur at a critical atom number [13]

$$N_c^0 = \frac{\pi^2}{6} \left(\frac{k_{\text{B}}T}{\hbar\omega_r} \right)^2. \quad (1)$$

This ideal-gas BEC transition is similar to the familiar condensation in 3d; it is purely statistical and follows from Einstein’s standard argument of the saturation of the excited states. However, the importance of dimensionality emerges if interactions are introduced. In 3d, ideal-gas BEC occurs when in the trap centre $D \approx 2.612$; weak interactions slightly shift the critical atom number [29–31], but do not alter the BEC-like nature of the transition. In 2d, while N_c^0 is finite, the phase-space density required in the trap centre for the excited states to saturate is infinite, just as in a uniform system [13]. For any $\tilde{g} > 0$ this is unattainable and the excited states can

accommodate any number of particles [32]. The BEC transition is thus suppressed and one expects it to be replaced by the BKT transition with non-infinite D_{BKT} [9].

These arguments suggest that the two conceptually very different phase transitions, the interaction-driven BKT and the saturation-driven BEC, are in fact continuously connected as $\tilde{g} \rightarrow 0$ [9, 33]. The harmonic trapping potential offers the opportunity to experimentally observe this unification of BKT and BEC physics. While in an infinite uniform gas no transition occurs for $\tilde{g} = 0$, in a harmonic trap a transition always occurs at a finite N_c and always results in significantly extended coherence of the gas. The nature of this transition is quantitatively encoded in the value of N_c . This picture is supported by theoretical calculations of the critical atom number N_c^{BKT} for a harmonically trapped gas [9, 34], which suggest that N_c^{BKT} smoothly connects to N_c^0 in the limit $\tilde{g} = 0$.

Various signatures of a phase transition, including emergence of extended coherence [14, 16–18, 20] and superfluidity [23], have been observed in trapped 2d gases with different specific \tilde{g} values. On the other hand, systematic studies with tuneable \tilde{g} have focussed on in-situ measurements of the equation of state [21, 26], which do not directly reveal any striking signatures of the infinite-order BKT transition.

In this Letter, we systematically study the critical point for the emergence of extended coherence in a harmonically trapped 2d Bose gas over a wide range of interaction strengths, $0.05 < \tilde{g} < 0.5$. We show, without any free parameters, that N_c generally agrees very well with the beyond-mean-field calculation of N_c^{BKT} [34], and converges onto N_c^0 of Eq. (1) as $\tilde{g} \rightarrow 0$. The critical chemical potential, μ_c , which directly reveals uniform-system conditions for a phase transition to occur in the trap centre, also agrees with the BKT theory and converges onto the BEC value, $\mu_c = 0$, for $\tilde{g} \rightarrow 0$. Our measurements also reiterate the importance of the suppression of density fluctuations in the normal state near the BKT critical point, previously observed in [17, 18, 20–22].

The experiment was carried out using a ^{39}K gas, in the apparatus described in [35]. For 2d trapping, the tight axial (vertical) confinement is provided by two repulsive “blades” of blue-detuned light, formed by passing a 532-nm gaussian beam through a $0-\pi$ phase-plate [19], while a red-detuned 1064-nm dipole trap provides the in-plane (horizontal) con-

finement. The radial and axial trapping frequencies are $(\omega_r, \omega_z) \approx 2\pi \times (38, 4100)$ Hz. For all our measurements $T \in [140 \text{ nK}, 190 \text{ nK}]$ and $\mu/k_B < 100 \text{ nK}$, resulting in a small ($< 30\%$) occupation of the excited axial states. The interaction strength, $\tilde{g} = \sqrt{8\pi}a/\ell_z$ [13], where a is the s-wave scattering length and $\ell_z = \sqrt{\hbar/(m\omega_z)}$, is controlled via a Feshbach resonance centred at 402.5 G [35, 36].

To characterise long-range coherence of a gas we study its (in-plane) momentum distribution $n(k)$ [18]. A change in the functional form of $g_1(r)$ leads to a dramatic change in its values at distances much larger than the thermal wavelength $\lambda = h/\sqrt{2\pi mk_B T}$ [13], and an increase of coherence over some large distance L manifests itself in enhanced population of the low-momentum states $k \lesssim 2\pi/L$. Thus, unlike the in-trap density distribution, which varies very smoothly through the BKT critical point [17, 18, 21, 22], $n(k)$ can provide a dramatic signature of the phase transition [18].

As illustrated in Fig. 1, to identify the critical point for a given \tilde{g} , we start with a highly coherent 2d gas and measure $n(k)$ after holding the cloud in the trap for a variable time t . During the hold time, the atom number N slowly decays through various inelastic processes [37], while the elastic-collision rate ($\approx 0.1 N \tilde{g}^2 \text{ s}^{-1}$) remains sufficiently high to ensure that the gas is in quasi-static equilibrium. To measure $n(k)$, we employ the ‘‘momentum focussing’’ technique [18, 28, 38, 39]: we turn off just the tight z confinement, so the rapid vertical expansion removes all the interaction energy on a timescale $1/\omega_z \ll 1/\omega_r$, and the subsequent horizontal evolution in the remaining in-plane harmonic potential reveals $n(k)$ as the spatial distribution after a quarter of the trap period. We probe this distribution by absorption imaging along z [see Fig. 1(a)].

Our k -space imaging resolution, $\Delta k \approx 0.4 \mu\text{m}^{-1}$, sets the largest distance over which we can probe coherence to $L = 2\pi/\Delta k \approx 15 \mu\text{m}$, which is much larger than $\lambda \approx 0.7 \mu\text{m}$. To probe coherence on this lengthscale, we simply monitor the peak value of the momentum distribution, P_0 , without making any theoretical assumptions about the exact shape of $n(k)$ at low k . To get the corresponding atom number N we do a simple summation over the image. Importantly, we eliminate the systematic error due to the uncertainty in the absorption-imaging cross section by independently calibrating our imaging system through measurements of the BEC critical point in a 3d gas [40].

In Fig. 1(b) we show a typical evolution of P_0 and N (here $\tilde{g} = 0.28$). While N decays smoothly, P_0 shows two distinct regimes, which allows us to identify the critical hold time t_c and the corresponding N_c . We note that $n(k)$ is narrower than a Gaussian even for N significantly below N_c , indicating some coherence on a lengthscale $> \lambda$ [13, 17, 20]. The smooth evolution of such non-Gaussian ‘‘peakiness’’ of $n(k)$ does not reveal a phase transition [20], and only P_0 corresponding to $L \gg \lambda$ shows a clear change in behaviour at a well-defined N_c [41]. Our large L is still small compared to the thermal diameter of the cloud, $2\sqrt{k_B T/(m\omega_r^2)} \approx 50 \mu\text{m}$, so the observed N_c is closely linked to the occurrence of a

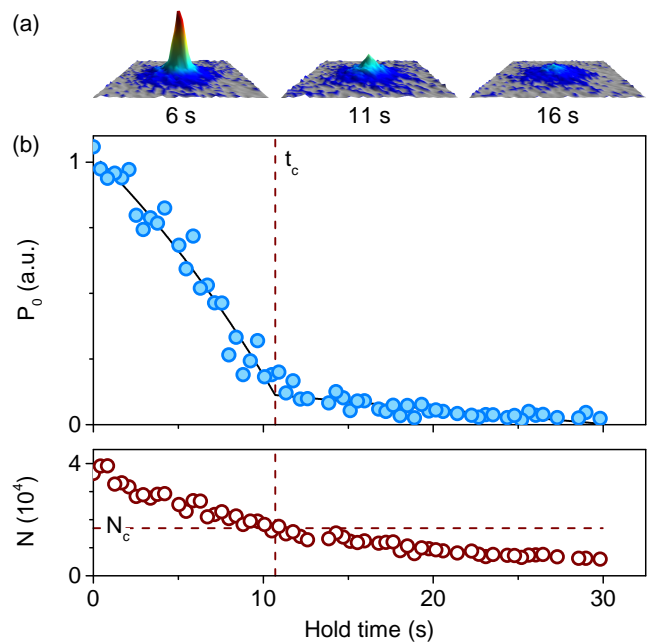


FIG. 1. (color online) Determination of the critical point for the onset of coherence, for $\tilde{g} = 0.28$ and $T \approx 140 \text{ nK}$. (a) Evolution of the momentum distribution, $n(k)$, with the hold time t (see text). Extended coherence is revealed as a sharp peak in $n(k)$. Each image is an average of three experimental realisations. (b) Evolution of the momentum-distribution peak, P_0 , and the smoothly decaying total atom number N . We associate the threshold-like behaviour of P_0 with the critical time t_c and deduce the corresponding N_c . The solid line is a heuristic piecewise fit function used to determine t_c [40].

phase transition in the centre of the trap [40].

For comparisons with theory, we also fit μ and T to each $n(k)$ image. Unlike in 3d, in 2d interactions affect $n(k)$ appreciably even in the normal state, and near the critical point it is in general insufficient to treat them at a mean-field (MF) level. However, beyond-MF correlations primarily affect the highly-populated low- k states [34]. We restrict our fits to the high- k wings of the distribution ($\hbar^2 k^2 > 2\tilde{g}mk_B T$), where we expect the beyond-MF effects to be small, and still carefully include the effects of interactions at a MF level [40]. Following [33], we also account for the residual thermal occupation of the axial excited states and the interaction-induced deformation of the axial eigenstates.

In Fig. 2 we summarise our measurements of the critical atom number for a wide range of interaction strengths. To compare our data with the strictly-2d theoretical calculations, we correct the observed ‘‘raw’’ N_c by subtracting the calculated population of the excited axial states [40]. We scale this corrected critical number, \tilde{N}_c , to the BEC critical atom number, N_c^0 of Eq. (1), and plot it versus \tilde{g} . Our Δk -limited value of L imposes a lower bound on \tilde{g} for which we can reliably identify the critical point. In the absence of any phase transition, in a weakly-interacting degenerate gas $g_1(r) \sim \exp(-r/\ell_0)$, with $\ell_0 = \lambda \exp(D/2)/\sqrt{4\pi}$ [13].

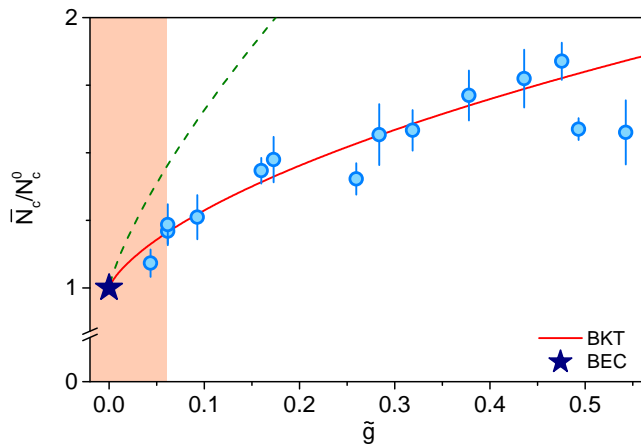


FIG. 2. (color online) Critical atom number as a function of the interaction strength \tilde{g} . All numbers are scaled to the ideal-gas BEC critical number N_c^0 , defined in Eq. (1). Solid line is the BKT prediction of Eq. (2), without any free parameters. Dashed line is an approximation which neglects suppression of density fluctuations in the normal state. The star (\star) denotes the critical point for BEC, which only occurs in the ideal-gas limit. The shaded region, $\tilde{g} < 0.06$, indicates the regime in which our measurements stop being reliable (see text). Error bars are statistical.

We thus do not expect our measurements to reliably identify N_c if $\ell_0 > L$ for some $D < D_{\text{BKT}}$. This occurs for $\tilde{g} < 380 \lambda^2 / (4\pi L^2) \approx 0.06$, indicated by the shaded area in Fig. 2 [42]. Our measurements also stop being reliable for $\tilde{g} \gtrsim 0.5$; in that regime our MF temperature fits are restricted to very high k values, which are affected by the anharmonicity of the optical trap. The error bars in Fig. 2 are statistical, while the systematic uncertainty in \tilde{N}_c/N_c^0 is $\lesssim 0.2$ [40].

Without any free parameters, we find generally excellent agreement with the BKT prediction of Ref. [34]:

$$\frac{N_c^{\text{BKT}}}{N_c^0} \approx 1 + \frac{3\tilde{g}}{\pi^3} \ln^2\left(\frac{\tilde{g}}{16}\right) + \frac{6\tilde{g}}{16\pi^2} \left[15 + \ln\left(\frac{\tilde{g}}{16}\right)\right], \quad (2)$$

which is based on fixing the phase-space density in the trap centre to D_{BKT} and integrating a uniform-system equation of state over the trap, using classical-field results of Ref. [44].

This agreement strongly supports the interpretation that the emergence of extended coherence corresponds to the BKT transition occurring in the central region of the trap. Moreover, the agreement with Eq. (2) over a very broad range of interaction strengths, and the proximity of our lowest reliable \tilde{g} values to zero, allow us to conclude that the critical atom number, without any free parameters, indeed smoothly converges onto the BEC result of Eq. (1).

It is instructive to also compare our data with the approximation $N_c^{\text{BKT}}/N_c^0 = 1 + 3\tilde{g}D_{\text{BKT}}^2/\pi^3$ [9, 11], shown by the dashed line in Fig. 2. Here, the critical phase-space density is again set to D_{BKT} , but the suppression of bosonic fluctuations in the normal state is neglected, i.e. the density profile is calculated using MF theory with an interaction potential $2gn(r)$, where $g = (\hbar^2/m)\tilde{g}$. Our data strongly exclude this result,

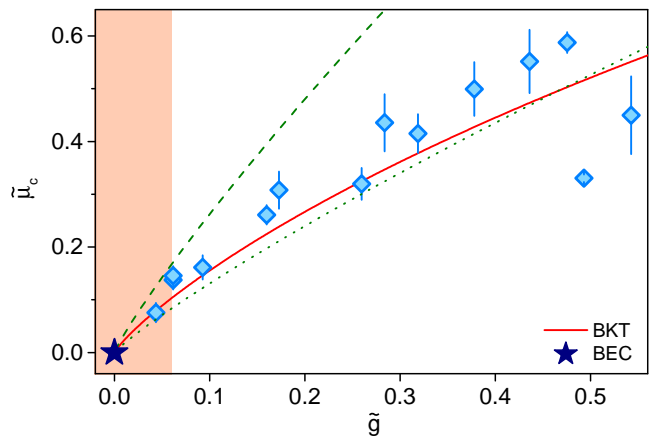


FIG. 3. (color online) Critical chemical potential as a function of the interaction strength \tilde{g} . Solid line is the classical-field BKT prediction. Dashed line is derived assuming a fully fluctuating Bose gas, while dotted line corresponds to a complete suppression of density fluctuations. Error bars are statistical.

confirming the importance of the suppression of density fluctuations near the critical point even for our lowest \tilde{g} values.

For a more direct comparison with the uniform-system BKT theory, we also consider the critical chemical potential for the onset of coherence. Like N_c in Fig. 1, μ_c is experimentally defined via the critical hold time t_c . The classical-field simulations [7] predict D_{BKT} to be reached for $\mu_c^{\text{BKT}} = k_B T (\tilde{g}/\pi) \ln(13.2/\tilde{g})$, which reduces to the BEC prediction, $\mu_c = 0$, for $\tilde{g} = 0$.

In Fig. 3 we plot $\tilde{\mu}_c = \mu_c/(k_B T)$ versus \tilde{g} , and again observe generally good agreement with the BKT theory (solid line), all the way down to $\tilde{g} \approx 0.06$, i.e. very close to the expected BEC limit. The small systematic difference between the data and the theory is comparable to our systematic uncertainty in $\tilde{\mu}_c$, of ~ 0.05 [40].

We also compare our data with two intuitive approximations to $\tilde{\mu}_c$. We consider interaction potentials γgn with $\gamma = 2$, corresponding to a fully fluctuating Bose gas, and $\gamma = 1$, corresponding to a complete suppression of density fluctuations. In both of these extremes one can analytically write $D_\gamma(\tilde{\mu}) = -\ln[1 - \exp(\tilde{\mu} - \gamma gn/(k_B T))]$ [13]. Defining $\tilde{\mu}_c^\gamma$ so that $D_\gamma(\tilde{\mu}_c^\gamma) = D_{\text{BKT}}$ we obtain the dashed ($\gamma = 2$) and dotted ($\gamma = 1$) lines in Fig. 3. Generally $\gamma = 1$ provides a better approximation, highlighting how strong the suppression of density fluctuations in the normal state is (see also [17, 18, 20–22]).

Finally, we note that in previous experiments [21, 26], on the in-trap equation of state, $\tilde{\mu}_c$ was deduced by defining it so as to satisfy the theoretical expectation [7, 44] that the phase-space density should be a universal function of $(\tilde{\mu} - \tilde{\mu}_c)/\tilde{g}$. Our measurements of $\tilde{\mu}_c$ defined through the emergence of extended coherence show that the two definitions indeed lead to very similar values.

In conclusion, by studying the critical point for the emer-

gence of extended coherence in a harmonically trapped 2d gas with tuneable interactions, we have quantitatively confirmed the predictions based on BKT theory and the expected unification of BKT and BEC transitions in the limit of vanishing interactions. The in-plane harmonic potential enables the observation of this unification. However, to quantitatively study the exact functional form of the slowly decaying correlations in a BKT superfluid, in the future it would be very interesting to study coherence of a tuneable 2d gas in a uniform potential [45–47]. Just below T_c this should reveal an interaction-strength-independent algebraic decay of the first-order correlation function, corresponding to a universal jump in the superfluid density [48].

We thank Naaman Tammuz and Alex Gaunt for experimental contributions in the early stages of the project, Shannon Whitlock for help with image processing, and Andre Wenz, Markus Holzmann and Jean Dalibard for useful discussions. This work was supported by AFOSR, ARO, DARPA OLE, and EPSRC [Grant No. EP/K003615/1]. N.N. acknowledges support from Trinity College, Cambridge, R.P.S. from the Royal Society, and K.V. from DAAD.

* These two authors contributed equally.

† rjf45@cam.ac.uk

‡ mrdsv2@cam.ac.uk

-
- [1] R. E. Peierls, *Surprises in Theoretical Physics* (Princeton University Press, Princeton, 1979).
- [2] N. N. Bogoliubov, *Physica* **26**, S1 (1960).
- [3] P. C. Hohenberg, *Phys. Rev.* **158**, 383 (1967).
- [4] N. D. Mermin and H. Wagner, *Phys. Rev. Lett.* **17**, 1133 (1966).
- [5] V. L. Berezinskii, *Soviet Physics JETP* **34**, 610 (1971).
- [6] J. M. Kosterlitz and D. J. Thouless, *J. Phys. C: Solid State Physics* **6**, 1181 (1973).
- [7] N. V. Prokof'ev, O. Ruebenacker, and B. V. Svistunov, *Phys. Rev. Lett.* **87**, 270402 (2001).
- [8] \tilde{g} is defined so that the strength of contact interactions is $g = \hbar^2 \tilde{g}/m$, where m is the atomic mass.
- [9] M. Holzmann, G. Baym, J. P. Blaizot, and F. Laloë, *P.N.A.S.* **104**, 1476 (2007).
- [10] S. T. Bramwell and P. C. W. Holdsworth, *Phys. Rev. B* **49**, 8811 (1994).
- [11] M. Holzmann and W. Krauth, *Phys. Rev. Lett.* **100**, 190402 (2008).
- [12] R. N. Bisset, M. J. Davis, T. P. Simula, and P. B. Blakie, *Phys. Rev. A* **79**, 033626 (2009).
- [13] Z. Hadzibabic and J. Dalibard, *Rivista del Nuovo Cimento* **34**, 389 (2011).
- [14] Z. Hadzibabic *et al.*, *Nature* **441**, 1118 (2006).
- [15] V. Schweikhard, S. Tung, and E. A. Cornell, *Phys. Rev. Lett.* **99**, 030401 (2007).
- [16] P. Krüger, Z. Hadzibabic, and J. Dalibard, *Phys. Rev. Lett.* **99**, 040402 (2007).
- [17] P. Cladé *et al.*, *Phys. Rev. Lett.* **102**, 170401 (2009).
- [18] S. Tung *et al.*, *Phys. Rev. Lett.* **105**, 230408 (2010).
- [19] S. P. Rath *et al.*, *Phys. Rev. A* **82**, 013609 (2010).
- [20] T. Plisson *et al.*, *Phys. Rev. A* **84**, 061606 (2011).
- [21] C.-L. Hung, X. Zhang, N. Gemelke, and C. Chin, *Nature* **470**, 236 (2011).
- [22] T. Yefsah *et al.*, *Phys. Rev. Lett.* **107**, 130401 (2011).
- [23] R. Desbuquois *et al.*, *Nat. Phys.* **8**, 645 (2012).
- [24] J.-y. Choi, S. W. Seo, W. J. Kwon, and Y.-i. Shin, *Phys. Rev. Lett.* **109**, 125301 (2012).
- [25] J.-y. Choi, S. W. Seo, and Y.-i. Shin, *Phys. Rev. Lett.* **110**, 175302 (2013).
- [26] L.-C. Ha *et al.*, *Phys. Rev. Lett.* **110**, 145302 (2013).
- [27] R. Desbuquois *et al.*, *Phys. Rev. Lett.* **113**, 020404 (2014).
- [28] M. G. Ries *et al.*, arXiv:1409.5373 (2014).
- [29] F. Dalfovo, S. Giorgini, L. P. Pitaevskii, and S. Stringari, *Rev. Mod. Phys.* **71**, 463 (1999).
- [30] F. Gerbier *et al.*, *Phys. Rev. Lett.* **92**, 030405 (2004).
- [31] R. P. Smith, R. L. D. Campbell, N. Tammuz, and Z. Hadzibabic, *Phys. Rev. Lett.* **106**, 250403 (2011).
- [32] Here we neglect the effects of the finite system size. Due to the non-zero spacing of the trap energy levels, $\hbar\omega_r$, the infinite D_{BEC} is replaced by a very large but finite non-universal value [13]. Consequently, the saturation-driven BEC can still occur for a range of extremely small but non-zero \tilde{g} values, $\tilde{g} \ll 10^{-2}$. This effect is not relevant for our measurements and conclusions.
- [33] Z. Hadzibabic *et al.*, *New J. Phys.* **10**, 045006 (2008).
- [34] M. Holzmann, M. Chevallier, and W. Krauth, *Phys. Rev. A* **81**, 043622 (2010).
- [35] R. L. D. Campbell *et al.*, *Phys. Rev. A* **82**, 063611 (2010).
- [36] G. Roati *et al.*, *Phys. Rev. Lett.* **99**, 010403 (2007).
- [37] These include collisions with the background gas in the vacuum chamber, three-body recombination, and scattering of photons from the trapping beams.
- [38] I. Shvarchuck *et al.*, *Phys. Rev. Lett.* **89**, 270404 (2002).
- [39] P. A. Murthy *et al.*, *Phys. Rev. A* **90**, 043611 (2014).
- [40] See *Supplemental Information* for details of image analysis, absolute atom-number calibration, fitting procedures, k -space resolution, and systematic errors.
- [41] If we probe coherence on a lengthscale $L' < L$, obtaining P'_0 by summing $n(k)$ up to $k' > \Delta k$, the change in the slope of P'_0 at t_c progressively gets washed out for decreasing L' .
- [42] Moreover, for $\tilde{g} < 0.05$ the elastic-collision rate ($\propto \tilde{g}^2$) is not sufficiently high for the gas to maintain thermal equilibrium [31, 43].
- [43] A. L. Gaunt, R. J. Fletcher, R. P. Smith, and Z. Hadzibabic, *Nat. Phys.* **9**, 271 (2013).
- [44] N. V. Prokof'ev and B. V. Svistunov, *Phys. Rev. A* **66**, 043608 (2002).
- [45] A. L. Gaunt *et al.*, *Phys. Rev. Lett.* **110**, 200406 (2013).
- [46] L. Corman *et al.*, *Phys. Rev. Lett.* **113**, 135302 (2014).
- [47] L. Chomaz *et al.*, arXiv:1411.3577 (2014).
- [48] D. R. Nelson and J. M. Kosterlitz, *Phys. Rev. Lett.* **39**, 1201 (1977).

Unification of BKT and BEC Phase Transitions in a Trapped Two-Dimensional Bose Gas

Supplemental Information

Richard J. Fletcher*, Martin Robert-de-Saint-Vincent*,

Jay Man, Nir Navon, Robert P. Smith, Konrad Viebahn, and Zoran Hadzibabic

Cavendish Laboratory, University of Cambridge, J. J. Thomson Avenue, Cambridge CB3 0HE, United Kingdom

Absorption image analysis

Fringe removal: Optical density (OD) images are usually affected by fringes due to the temporal variations in the probe intensity. We eliminate this effect using the fringe-removal algorithm of Ockeloen *et al.* [1].

Imaging at high magnetic field: Near the Feshbach resonance our atoms are in the electronic ground state approximately described by $|4S_{1/2}, m_J = -1/2, I = 3/2, m_I = 3/2\rangle$, and are imaged on the transition to the excited state $|4P_{3/2}, m_J = -3/2, I = 3/2, m_I = 3/2\rangle$. However, due to the residual hyperfine mixing in the ground state manifold, the imaging transition is not perfectly cycling, and the probability of optical pumping into other ground states is $\approx 3\%$ per cycle. Consequently, the relation between the observed OD and the atomic column density depends on the number of photons scattered per atom, which in turn varies with the inhomogeneities of the probe beam.

To correct for this effect, we experimentally calibrate the relative variation of the observed OD(\vec{r}) with the camera counts, $C(\vec{r})$, in the reference image taken without atoms. For this, we image a 3d thermal cloud after expansion from a dipole trap. Assuming cylindrical symmetry of the cloud, any variations in OD observed along a ring concentric with the cloud centre we attribute to the variations in the probe intensity. Averaging over several images, we build, pixel by pixel, a correlation plot of OD/OD₀ versus C/C_0 , where C_0 is a fixed reference value and OD₀ the corresponding optical density. We construct such plots for various ring radii (i.e. various atomic column densities) and various (mean) probe intensities, and find that to a very good approximation the scaling of the optical density due to the optical pumping depends only on the light intensity and not on the atomic column density. We thus finally create an interpolated rescaling function $F(C/C_0) = \text{OD}_0/\text{OD}$, and correct our images according to $\text{OD}_{\text{scaled}}(\vec{r}) = \text{OD}(\vec{r}) \cdot F(C(\vec{r})/C_0)$. This relative calibration corrects for both the optical pumping and for the Doppler shifting of atoms with increasing number of scattering events.

Imaging-intensity optimisation: In our main experimental sequences we take two sets of interlaced images, under identical conditions, but with two different (mean) imaging-beam intensities: a “low” intensity $I_0 \approx 0.08 \text{ mW/cm}^2$ and a “high” intensity $I_1 \approx 0.3 \text{ mW/cm}^2$ (which is still well below the saturation intensity $I_{\text{sat}} \approx 1.8 \text{ mW/cm}^2$), for which the scaling function F is larger by a factor of 2.7. The low-intensity images are used for determining N , T and μ , while

the high-intensity images are used just to determine, with a larger dynamic range, the high-OD momentum peak P_0 .

Absolute atom-number calibration

To calibrate our absolute imaging detectivity, we measure the BEC critical point in a 3d gas [2], prepared in an optical dipole trap of frequencies $(\omega_x, \omega_y, \omega_z) = 2\pi \times (64.3(1.0), 54.0(6), 93.9(2)) \text{ Hz}$. We calibrate the observed critical atom number on the theoretical value:

$$N_c = A \frac{N_c^{\text{ideal}}}{[1 - 3.426(a/\lambda) + 42(a/\lambda)^2]^3} + \delta N_c^{\text{fs}}. \quad (1)$$

Here, $N_c^{\text{ideal}} = \zeta(3)(k_B T)^3 / (\hbar^3 \omega_x \omega_y \omega_z)$, where ζ is the Riemann function, the denominator in Eq. (1) corresponds to mean-field (MF) and beyond-MF corrections [2], $A \approx 1.1$ is the trap-anharmonicity correction for our Gaussian potential, and δN_c^{fs} is the finite size-correction [3]. For probe intensity I_0 and image-pulse duration of 80 μs we obtain an effective absorption cross section $\sigma_{\text{eff}} = 0.25(1) \times 3\lambda_0^2 / (2\pi)$, where $\lambda_0 \approx 767 \text{ nm}$ is the imaging wavelength.

Extraction of thermodynamic parameters

Model functions: To extract μ and T from our images, we fit a model to the azimuthally-averaged momentum distributions. By constraining the fit to the wings where $\hbar^2 k^2 > 2mk_B T \tilde{g}$, we ensure that interaction effects are described well within a mean-field (MF) framework [4].

The model we use includes the thermal occupation of the excited axial states and the interactions between atoms in all axial states, as in [5, 6], and also the axial deconfinement of the cloud due to the repulsive interactions, as in [7].

We construct the model 2d momentum distribution for an in-plane potential $V(x, y)$ within the 2d local density approximation. Defining the local chemical potential $\mu_L(x, y) = \mu - V(x, y)$, and writing $\vec{r} = (x, y)$, we have

$$n(\vec{k}) = \sum_j \int d^2 r \left[\exp \left(\frac{\frac{\hbar^2 k^2}{2m} + \varepsilon_j(\vec{r}) - \mu_L(\vec{r})}{k_B T} \right) - 1 \right]^{-1}, \quad (2)$$

where $\{\varepsilon_j\}(\vec{r})$ are the eigenenergies of the axial states of motion, $\{\phi_j(z)\}(\vec{r})$. Due to interactions, they are not simply $\hbar\omega_z(j + 1/2)$, but depend on $\mu_L(\vec{r})$.

	Statistical	Systematics		
		Calibration	Finite size	Anharmonicity
\bar{N}_c/N_c^0	± 0.08	± 0.14	$+0.04$	-0.01
$\tilde{\mu}_c$	± 0.03	± 0.05	$+0.005$	-0.04

TABLE I. Absolute standard uncertainties (68% confidence interval) and estimated systematic shifts affecting the measured \bar{N}_c/N_c^0 and $\tilde{\mu}_c$. Statistical errors are shown as error bars in the main paper. All values are typical for the experimentally explored range of \tilde{g} . The positive (negative) systematic shifts correspond to the measured values being higher (lower) than the true ones.

To evaluate the set $\{\varepsilon_j\}(\mu_L)$ we solve the 1d axial problem defined by two coupled equations:

$$n_3(z) = -\frac{1}{\lambda^2} \sum_j \ln \left[1 - \exp \left(\frac{\mu_L - \varepsilon_j}{k_B T} \right) \right] |\phi_j(z)|^2, \quad (3)$$

where n_3 is 3d density, and

$$\left[\frac{-\hbar^2}{2m} \frac{d^2}{dz^2} + \frac{1}{2} m \omega_z^2 z^2 + 2g_3 n_3(z) \right] \phi_j(z) = \varepsilon_j \phi_j(z), \quad (4)$$

where $g_3 = 4\pi\hbar^2 a/m$. We iteratively find a self-consistent solution to Eqs. (3-4), and then compute $n(\vec{k})$ in Eq. (2).

Critical parameters: To identify the critical time t_c , we fit the following heuristic function to $P_0(t)$:

$$P_0(t) = P_c + \Theta(t - t_c) \cdot c \cdot |t - t_c| + \Theta(t_c - t) \cdot a [1 - \exp(-b|t - t_c|)], \quad (5)$$

where $\Theta(t)$ is the Heaviside function. In the limit $b \ll 1/|t - t_c|$, this is simply a piecewise linear function, while the non-zero b allows for the saturation of the peak OD at short t .

To determine $N(t_c)$, $T(t_c)$ and $\mu(t_c)$ we fit the smooth time evolutions of N , T and μ by third-order polynomials.

Finally, we use the above MF model to compute the occupations of the $j > 0$ axial states for $(T(t_c), \mu(t_c))$, and correct N_c to get \bar{N}_c . This operation assumes that beyond-MF effects affect only the axial ground state. This approximation is justified by the fact that $\hbar\omega_z/k_B T > \tilde{g}$ [4].

Momentum-space resolution

Our k -space resolution is limited by the camera pixel size and by the slight anisotropy of the in-plane harmonic potential in which we perform the momentum focusing. After removing the green “blade” beams, we have $\omega_{x,y} = \bar{\omega} \pm \Delta\omega$, with $\bar{\omega}/(2\pi) = 36.3(1)$ Hz and $\Delta\omega/(2\pi) = 2.5(1)$ Hz. This means that the focusing is not obtained simultaneously in both directions, but at the focusing time $t_f = \pi/(2\bar{\omega}) \approx 7$ ms the blurring of the momentum distribution is isotropic, with

$\Delta k \approx \sqrt{mk_B T/\hbar^2} \sin(\Delta\omega t_f) \approx 0.4 \mu\text{m}^{-1}$. This happens to closely coincide with the resolution set by the pixel size. To determine the height of the momentum peak, P_0 , we average the image within one pixel of the fitted cloud centre.

Confidence intervals

In Table I, we summarise the main uncertainties in the critical parameters \bar{N}_c/N_c^0 and $\tilde{\mu}_c$ in Figs. 2-3 in the main paper.

The statistical errors, defined as 68% confidence interval and arising from experimental noise and fitting errors, are shown by the error bars in the main paper. Here they are averaged over the experimental points.

Systematic uncertainties in Table I fall into three categories: (i) calibration errors and drifts in the trapping frequencies, imaging magnification and absolute detectivity, (ii) finite-size (non-zero ω_r) effects, and (iii) anharmonicity of the optical trapping potentials. These affect the calculated N_c^0 and also the model functions used for extracting μ and T . The calibration errors we calculate by propagating errors, the finite-size effects are calculated following [3], and we assess the typical magnitude of the anharmonicity shifts by numerical simulations in the ideal-gas limit.

Additionally, two more fundamental systematic effects could shift the apparent critical point. If we assume that the emergence of coherence over lengthscale L requires the whole region near the cloud centre, of radius $L/2$, to be superfluid, then the trap inhomogeneity leads to apparent positive shifts of \bar{N}_c/N_c^0 and $\tilde{\mu}_c$, of $\lesssim 0.2$ and ≈ 0.05 , respectively. On the other hand, the critical divergence of the correlation length above T_c has an opposite effect, which we estimate to be of comparable absolute size [8]. We thus expect these two effects to partially cancel, and lead to overall shifts that do not exceed our statistical and systematic errors (see also [9]).

-
- [1] C. Ockeloen, A. Tauschinsky, R. Spreuw, and S. Whitlock, Phys. Rev. A **82**, 061606 (2010).
 - [2] R. P. Smith, R. L. D. Campbell, N. Tammuz, and Z. Hadzibabic, Phys. Rev. Lett. **106**, 250403 (2011).
 - [3] T. Haugset, H. Haugerud, and J. O. Andersen, Phys. Rev. A **55**, 2922 (1997).
 - [4] M. Holzmann, M. Chevallier, and W. Krauth, Phys. Rev. A **81**, 043622 (2010).
 - [5] R. N. Bisset, D. Baillie, and P. B. Blakie, Phys. Rev. A **79**, 013602 (2009).
 - [6] S. Tung *et al.*, Phys. Rev. Lett. **105**, 230408 (2010).
 - [7] Z. Hadzibabic *et al.*, New J. Phys. **10**, 045006 (2008).
 - [8] Z. Hadzibabic and J. Dalibard, Rivista del Nuovo Cimento **34**, 389 (2011).
 - [9] R. N. Bisset, M. J. Davis, T. P. Simula, and P. B. Blakie, Phys. Rev. A **79**, 033626 (2009).